

A METHOD TO EXTRACT THE ANGULAR POWER SPECTRUM OF THE EPOCH OF REIONIZATION FROM LOW-FREQUENCY RADIO INTERFEROMETERS

QIAN ZHENG^{1,2}, XIANG-PING WU^{1,3}, JUN-HUA GU¹, JINGYING WANG³, AND HAIGUANG XU³*Draft version November 11, 2018*

ABSTRACT

The redshifted 21cm signal of neutral hydrogen from the epoch of reionization (EoR) is extremely weak and its first detection is therefore expected to be statistical with first-generation low-frequency radio interferometers. In this letter we propose a method to extract the angular power spectrum of EoR from the visibility correlation coefficients $p_{ij}(u, v)$, instead of the visibilities $V_{ij}(u, v)$ measured directly by radio interferometers in conventional algorithm. The visibility correlation coefficients are defined as $p_{ij}(u, v) = V_{ij}(u, v) / \sqrt{|V_{ii}||V_{jj}|}$ by introducing the auto-correlation terms V_{ii} and V_{jj} such that the angular power spectrum C_ℓ can be obtained through $C_\ell = 4\pi^2 T_0^2 \langle |p_{ij}(u, v)|^2 \rangle$, independently of the primary beams of antennas. This also removes partially the influence of receiver gains in the measurement of C_ℓ because the amplitudes of the gains cancel each other out in the statistical average operation of $\langle |p_{ij}(u, v)|^2 \rangle$. The average brightness temperature T_0 of extragalactic sources is used as the calibrator of C_ℓ . Finally we demonstrate the feasibility of the novel method using the simulated sky maps as targets and the 21 CentiMeter Array (21CMA) as interferometer.

Subject headings: cosmology: theory — diffuse radiation — intergalactic medium — methods: data analysis — techniques: interferometric

1. INTRODUCTION

While the redshifted 21cm emission/absorption of neutral hydrogen provides a unique cosmological probe of the epoch of reionization (EoR) -, the last frontier of observational cosmology, there are two primary challenges of measuring the EoR signatures with most of the dedicated radio facilities (e.g., 21CMA, LOFAR, LWA, MWA, PAPER, SKA, etc.): First, the cosmic signal from EoR is deeply buried under the extremely bright foreground dominated by our Galaxy, extragalactic sources and telescope noise, and an unprecedented level of foreground removals down to five orders of magnitude should be required in order to detect the cosmic signal (e.g., Madau et al. 1997; Zaldarriaga et al. 2004). Second, low-frequency radio interferometric measurements in current 21cm experiments suffer from various instrumental contaminations in addition to man-made radio-frequency interference. Outstanding among these are the frequency-dependent point spread function and field-of-view (also known as 'mode-mixing'), complexity of calibration, and bright source subtraction (e.g., Morales et al. 2006; Liu et al. 2009; Bowman et al. 2009; Datta et al. 2009, 2010; Bernardi et al. 2010; Datta et al. 2010; Petrovic & Oh 2011). Yet, it is generally agreed among the 21cm cosmology community that the advent of many sophisticated techniques and algorithms in recent years helps overcoming these observational and technical hurdles, allowing to reach the desired detection sensitivity with the first generation of radio interferometers (for recent reviews see Furlanetto et al. 2006; Morales & Wyithe 2010; Pritchard & Loeb 2012; Zaroubi 2012).

The theoretically predicted brightness temperature of 21cm signal from EoR is only ~ 10 mK, and first capture of such extremely weak signal is therefore expected to be statistical (Zaldarriaga et al. 2004). Most of the current 21cm experiments aiming to detect the EoR signal are based on radio interferometric technique, which provides a direct measure of the Fourier component of the sky brightness $I(\mathbf{s})$ convolved with the primary beam of the antennas $B_{ij}(\mathbf{s})$ towards direction \mathbf{s} , often known as the visibility $V_{ij}(\mathbf{u})$ at a given baseline \mathbf{u} in units of wavelength:

$$V_{ij}(\mathbf{u}) = g_i g_j^* \int B_{ij}(\mathbf{s}) I(\mathbf{s}) e^{-2\pi i \mathbf{u} \cdot \mathbf{s}} d^2 \mathbf{s}, \quad (1)$$

where g_i and g_j are the complex gain factors of antenna pair i and j , respectively. It can be easily shown that the angular power spectrum (C_ℓ) of the sky brightness distribution $I(\mathbf{s})$ can be constructed by the average value of the square of $V_{ij}(\mathbf{u})$ with the Fourier wavenumber $\ell = 2\pi u$ (White et al. 1999). In particular, under the assumption that the angular power spectrum varies rather slowly with scale relative to the Fourier component of the primary beam $\tilde{B}_{ij}(\mathbf{u}) = \mathcal{F}[B_{ij}(\mathbf{s})]$, we obtain the commonly used formula in the estimation of the angular power spectrum of low-frequency sky at a given frequency (Bharadwaj & Sethi 2001; Zaldarriaga et al. 2004; Bharadwaj & Ali 2005; Santos et al. 2005; Ali et al. 2008; Pen et al. 2009; Paciga et al. 2011; Ghosh et al. 2011a, 2011b):

$$\langle |V_{ij}(\mathbf{u})|^2 \rangle \approx C_{\ell=2\pi u} |g_i|^2 |g_j|^2 \int d^2 \mathbf{u}' |\tilde{B}_{ij}(\mathbf{u} - \mathbf{u}')|^2. \quad (2)$$

However, most of the theoretical studies in literature implicitly assume that perfect calibrations are being made for radio interferometers, and gains and primary beam introduce no spectral and spatial structures to destroy the reconstruction of the EoR angular power spectrum.

¹ National Astronomical Observatories, Chinese Academy of Sciences, Beijing 100012, China

² Graduate School of Chinese Academy of Sciences, Beijing 100049, China

³ Department of Physics, Shanghai Jiao Tong University, 800 Dongchuan Road, Shanghai 200240, China

But in reality, to perform precise calibration in the existence of ionospheric turbulence and to maintain high stability of radio instruments for rather a long integration time are extremely difficult for current 21cm experiments. This motivates us in this Letter to explore a possible remedy to overcome some of these shortcomings by using the visibility correlation coefficients instead of the visibilities. With the novel method it will be possible to statistically extract the EoR angular power spectrum from radio interferometric measurements, independently of the primary beam of antennas. The method also allows us to remove partially the influence of receiver gains in the statistical measurement of C_ℓ because the amplitudes of the gains cancel each other out.

2. FORMALISM

We begin with the auto-correlation of voltages measured at each antenna, which corresponds to the visibility with baseline $\mathbf{u} = 0$:

$$|V_{ii}|^2 = |g_i|^4 I_0^2 \int d^2\mathbf{s} |B_{ii}(\mathbf{s})|^2. \quad (3)$$

This formula applies for discrete extragalactic sources only, and I_0 denotes the mean brightness of the point sources rather than the total power. The latter is dominated by the Milky Way in our interested frequency range below 200 MHz. Now we define the visibility correlation coefficient such that

$$p_{ij}(\mathbf{u}) = \frac{V_{ij}(\mathbf{u})}{\sqrt{|V_{ii}||V_{jj}|}}. \quad (4)$$

With this definition the amplitudes of the complex gains cancel each other out but the signal coherence remains. Following eq.(2) we take the average value of the square of $p_{ij}(\mathbf{u})$

$$\langle |p_{ij}(\mathbf{u})|^2 \rangle \approx \frac{C_{\ell=2\pi u}}{I_0^2} \frac{\int d^2\mathbf{u}' |\tilde{B}_{ij}(\mathbf{u} - \mathbf{u}')|^2}{\sqrt{\int d^2\mathbf{s} |B_{ii}(\mathbf{s})|^2 \int d^2\mathbf{s} |B_{jj}(\mathbf{s})|^2}}. \quad (5)$$

Using the 'frequency shift' theorem of the Fourier transform, we can rewrite the Fourier component of the primary beam $\tilde{B}_{ij}(\mathbf{u} - \mathbf{u}')$ as $\tilde{B}_{ij}(\mathbf{u} - \mathbf{u}') = \mathcal{F}[B_{ij}(-\mathbf{s})e^{-2\pi i\mathbf{u}\cdot\mathbf{s}}]$. According to the Parseval's theorem, the total power in the \mathbf{s} domain or the \mathbf{u}' domain should be the same. This yields

$$\frac{1}{4\pi^2} \int d^2\mathbf{u}' |\tilde{B}_{ij}(\mathbf{u} - \mathbf{u}')|^2 = \int d^2\mathbf{s} |B_{ij}(-\mathbf{s})e^{-2\pi i\mathbf{u}\cdot\mathbf{s}}|^2 = \int d^2\mathbf{s} |B_{ij}(-\mathbf{s})|^2. \quad (6)$$

The most crucial point of this equation, however, is that the power $\int d^2\mathbf{u}' |\tilde{B}_{ij}(\mathbf{u} - \mathbf{u}')|^2$ is actually independent of \mathbf{u} . Namely, in the conventional estimate of angular power spectrum from eq.(2) the primary beam term $\int d^2\mathbf{u}' |\tilde{B}_{ij}(\mathbf{u} - \mathbf{u}')|^2$ does not alter the shape of the power spectrum. This arises, of course, from the presumption that the primary beam varies rather slowly with angular scale relative to the cosmic signal, a necessary prerequisite for taking out from the integral the $C_{\ell=2\pi u}$ term in eq.(2). Furthermore, the symmetric feature of the primary beam for interferometric array

element in all the current 21cm experiments suggests that $B_{ij}(\mathbf{s})$ can be actually treated as an even function, implying $B_{ij}(-\mathbf{s}) = B_{ij}(\mathbf{s})$. Now, we apply the Cauchy-Schwarz inequality to the integral $\int d^2\mathbf{s} |B_{ij}(\mathbf{s})|^2$ by noticing $B_{ij}(\mathbf{s}) = B_i(\mathbf{s})B_j^*(\mathbf{s})$, $|B_i(\mathbf{s})|^2 = |B_{ii}(\mathbf{s})|$ and $|B_j(\mathbf{s})|^2 = |B_{jj}(\mathbf{s})|$, and obtain

$$\left| \int d^2\mathbf{s} |B_{ij}(\mathbf{s})|^2 \right|^2 = \left| \int d^2\mathbf{s} |B_{ii}(\mathbf{s})| |B_{jj}(\mathbf{s})| \right|^2 \leq \int d^2\mathbf{s} |B_{ii}(\mathbf{s})|^2 \int d^2\mathbf{s} |B_{jj}(\mathbf{s})|^2. \quad (7)$$

The equals sign holds when all antenna elements have identical primary beam $B_i(\mathbf{s}) = B_j(\mathbf{s})$. Finally, replacing the integral $\int d^2\mathbf{u}' |\tilde{B}_{ij}(\mathbf{u} - \mathbf{u}')|^2$ in eq.(5) by eqs.(6) and (7) and using again the Parseval's theorem we find

$$\frac{\int d^2\mathbf{u}' |\tilde{B}_{ij}(\mathbf{u} - \mathbf{u}')|^2}{\sqrt{\int d^2\mathbf{s} |B_{ii}(\mathbf{s})|^2 \int d^2\mathbf{s} |B_{jj}(\mathbf{s})|^2}} = 4\pi^2 \quad (8)$$

This allows us to evaluate the angular power spectrum C_ℓ relative to the mean brightness I_0 of point sources simply through

$$C_{\ell=2\pi u} = 4\pi^2 I_0^2 \langle |p_{ij}(\mathbf{u})|^2 \rangle. \quad (9)$$

Consequently, we may use the average sky brightness of extragalactic sources over the primary beam of the antenna as the reference or calibration. While many sophisticated models have been constructed for low frequency sky for the purpose of foreground removals in 21cm experiments (e.g. de Oliveira-Costa et al. 2008; Jelić et al. 2008; Wilman et al. 2008; Vernstrom et al. 2011; Kogut 2012), for our purpose a simple power-law as the global sky brightness temperature model of extragalactic sources should suffice to calibrate the angular power spectrum at each frequency ν : $T_0 = 13.7\text{K} \left(\frac{\nu}{150\text{MHz}}\right)^{-2.74}$. This is the best-fit mean sky temperature over a field of view of $20^\circ \times 20^\circ$ at the frequency range 100-200 MHz based on the numerical simulations by Wilman et al (2008) after bright sources with fluxes greater than 10 mJy at 150 MHz are removed (see Section 3). Note that C_ℓ will represent the angular power spectrum of the sky brightness temperature distribution if I_0 is replaced by T_0 in eq.(9): $C_{\ell=2\pi u} = 4\pi^2 T_0^2 \langle |p_{ij}(\mathbf{u})|^2 \rangle$.

3. SIMULATION TEST

In order to test the feasibility of extracting angular power spectrum of low-frequency sky with the novel method, we use the simulated sky maps by Wilman et al. (2008) as the input and the 21 CentiMeter Array (21CMA) as the radio interferometer. Following the same algorithm of Zheng et al. (2012), we generate a set of sky maps of $20^\circ \times 20^\circ$ for different frequencies, containing five distinct radio source types out to redshift of $z=20$. We estimate the flux of each radio source at different observing frequencies between 100 MHz and 200 MHz by a running power-law in frequency: $S \propto \nu^{\alpha+\Delta\alpha \lg(\nu/\nu_*)}$, in which ν_* is the characteristic frequency and is taken to be 150 MHz in this study. Finally, we exclude all the bright sources with fluxes $S_{150\text{MHz}}$ exceeding 10 mJy at 150 MHz which are assumed to be resolvable by current radio interferometers and can therefore be excised with

existing algorithms. We fix a 4096^2 grid for each of the simulated image, which gives rise to an angular resolution of $0'.3$ (see Figure 1).

21CMA, sited in Western China, is a ground-based meter-wave array designed to probe the EoR operating at frequencies from 50 MHz to 200 MHz. The array consists of 80 pods (or stations) with 127 log-period antennas for each, which are deployed in two perpendicular arms along east-west and north-south directions, respectively. Spacings between pods are integral multiples of 20 m, with a maximum baseline of 2740 m along each baseline. The 21CMA redundancy is being used for the purposes of not only calibrations but also statistical measurement of the angular power spectrum of EoR at specific modes. In this work we choose the 40 pods of the east-west arm to generate the uv sampling towards the north celestial pole region, which reduces significantly the computing complexity in visibilities $V_{i,j}(u, v)$ since only two-dimensional Fourier transform is involved for such a configuration. The corresponding baseline (i.e. uv sampling) distribution of the 780 pod pairs as interferometers for the 21CMA east-west arm is shown in Figure 2, among which there are only 127 independent baselines.

The simulated sky map is convolved with the 21CMA primary beam $B_i(\mathbf{s})$ which is identical for all the pods and takes approximately a Gaussian function with $\text{FWHM} = 4'.26(\nu/100\text{MHz})^{-1}$. We perform the Fourier transform of the simulated sky map modulated by $B_{ij}(\mathbf{s})$ to produce the uv map in terms of eq.(1) by setting $g_i = g_j = 1$. The uv map is further sampled by the 21CMA east-west baselines shown in Figure 2. We now calculate the visibility correlation coefficients $p_{ij}(u, v)$ at each frequency channel for all the 780 baselines. This yields a set of $p_{ij}(u, v)$ measures at 127 independent Fourier modes $\ell = 2\pi\sqrt{u^2 + v^2}$. Finally, the angular power spectra at these specific modes can be obtained using eq.(9), $C_{\ell=2\pi u} = 4\pi^2 T_0^2 \langle |p_{ij}(u, v)|^2 \rangle$, in which the average sky brightness temperature for our case is determined by the unresolved extragalactic sources $T_0 = 13.7\text{K}(\nu/150\text{MHz})^{-2.74}$ because the Galactic foreground has not been included in the simulation and the bright sources have been already removed.

Figure 3 shows the angular power spectra of the simulated sky maps at four frequencies ranging from 120 MHz to 180 MHz, together with the recovered ones at specific modes sampled by the 21CMA east-west baselines. The former are constructed directly using the Fourier transform of the simulated sky images without inclusion of any instrumental effects, while the latter are the reconstructed results from the 21CMA 'observations' based on the novel algorithm of eq.(9). It appears that the two results show a remarkably good agreement. We have also demonstrated the measurement errors assuming an integration time of 300 days, an observing bandwidth of 1 MHz and the system noise of 300 K. In particular, the noise level at C_ℓ has been suppressed by a factor of $1/\sqrt{N_\ell}$ for the redundant baseline of N_ℓ equally spaced pods. Large error bars at small- and large- ℓ ends can be attributed to the arcminute-scale angular resolution due to the short baselines and the cosmic variance due to the small field-of-view of the 21CMA, respectively. For comparison the reconstructed angular power spectra directly from Figure 1 are also plotted in Figure 3. It appears

that the Gaussian beam alters only the amplitude rather than the shape of the angular power spectrum in terms of eqs.(2) and (6). As is shown in Figure 3, such an amplitude effect has been corrected for when the visibility correlation coefficients $p_{ij}(u, v)$ are used. Yet, in practice the primary beam can hardly be modeled by a perfect Gaussian function or other form of simple analytical function. A careful calibration of the primary beam of antennas to a high degree of precision must be made. Imperfect and inaccurate calibrations of both spatial and spectral properties of the primary beam may lead to significant errors in reconstruction of the power spectrum of EoR for 21cm experiments. Employment of the visibility correlation coefficients in the statistical study of EoR allows us to eliminate concern about the calibration of the primary beam. While with our new algorithm we have successfully recovered the angular power spectra of the simulated radio foregrounds, the foregrounds should be eventually suppressed to the level below 10 mK, a minimum requirement for extracting statistically the signatures of EoR. This can be achieved, for example, using the foreground removal technique suggested recently by Cho et al.(2012), which works straightforwardly with the angular power spectrum. We have tested the technique and found that the foregrounds can indeed be subtracted to the level below 10 mK.

4. DISCUSSION AND CONCLUSIONS

Instead of directly employing the visibilities in conventional interferometric measurements of the statistical fluctuations of EoR suggested in literature, we propose to work with the visibility correlation coefficients defined by $p_{ij}(u, v) = V_{ij}(u, v)/\sqrt{|V_{ii}||V_{jj}|}$. This allows us to eliminate the effect of primary beams of antennas and also partially reduce the influence of receiver gains on the statistical extraction of the angular power spectrum of the low-frequency sky: $C_{\ell=2\pi u} = 4\pi^2 T_0^2 \langle |p_{ij}(u, v)|^2 \rangle$. Yet, we need to calibrate the power spectrum using the average brightness temperature T_0 of extragalactic sources for low-frequencies below 200 MHz. Observationally, T_0 has been determined so far to a degree of satisfaction at least for our purpose (e.g., Di Matteo et al. 2002).

Introduction of the visibility correlation coefficient $p_{ij}(u, v)$ does not change the coherence of original signal. Hence the phase correction such as self-calibration and/or redundant calibration should be still made before combining $p_{ij}(u, v)$ data. Furthermore, bright sources in the field-of-view have to be removed to reduce the Poisson noise in computation of the angular power spectrum. This also implies that the sidelobes of bright sources still remain as troublesome for reconstruction of angular power spectrum no matter whether $V_{ij}(u, v)$ or $p_{ij}(u, v)$ is used. Another reason that bright sources should be excised before recovery of the angular power spectrum is the requirement of uniformity assumption for taking out from the integral the angular power spectrum term C_ℓ in eq.(2).

We have tested the feasibility of the novel method using the simulated sky maps of $20^\circ \times 20^\circ$ for extragalactic sources in low-frequencies as the targets and 21CMA as the radio interferometer. We have successfully recovered the angular power spectra of the foregrounds at specific Fourier modes sampled by the 127 independent baselines of the 21CMA east-west arm, after the bright sources

with fluxes of $S_{150\text{MHz}} \geq 10$ mJy are removed. While we have not included the gain fluctuations in sampling of the visibilities, the new method does allow us to remove the effect of the spatial response of the 21CMA antennas on the reconstruction of the angular power spectrum of the low-frequency sky. In combination of various sophisticated foreground removal techniques developed in recent years especially in the power spectrum domain (e.g. Cho et al. 2012), we should be able to subtract the foreground to the level for statistical detection of the

21cm signal from EoR.

5. ACKNOWLEDGEMENTS

We gratefully acknowledge the constructive suggestions and insightful comments by the referee. In particular we would like to thank Abhik Ghosh for kindly pointing out an error in Eq.(3) in the first version of our manuscript. This work was supported by the Ministry of Science and Technology of China, under grant No. 2009CB824900

REFERENCES

- Ali, S. S., Bharadwaj, S., & Chengalur, J. N. 2008, MNRAS, 385, 2166
- Bernardi, G., de Bruyn, A. G., Harker, G., et al. 2010, A&A, 522, A67
- Bharadwaj, S., & Ali, S. S. 2005, MNRAS, 356, 1519
- Bharadwaj, S., & Sethi, S. K. 2001, J&A, 22, 293
- Bowman, J. D., Morales, M. F., & Hewitt, J. N. 2009, ApJ, 695, 183
- Cho, J., Lazarian, A., & Timbie, P. T. 2012, ApJ, 749, 164
- Datta, A., Bhatnagar, S., & Carilli, C. L. 2009, ApJ, 703, 1851
- Datta, A., Bowman, J. D., & Carilli, C. L. 2010, ApJ, 724, 526
- de Oliveira-Costa, A., Tegmark, M., Gaensler, B. M., et al. 2008, MNRAS, 388, 247
- Di Matteo, T., Perna, R., Abel, T., & Rees, M. J. 2002, ApJ, 564, 576
- Furlanetto, S. R., Oh, S. P., & Briggs, F. H. 2006, Phys. Rep. 433, 181
- Ghosh, A., Bharadwaj, S., Ali, S. S., & Chengalur, J. N. 2011a, MNRAS, 411, 2426
- Ghosh, A., Bharadwaj, S., Ali, S. S., & Chengalur, J. N. 2011b, MNRAS, 418, 2584
- Jelić V., Zaroubi, S., Labropoulos, P., et al. 2008, MNRAS, 389, 1319
- Kogut, A. 2012, ApJ, 753, 110
- Liu, A., Tegmark, M., Bowman, J., Hewitt, J., & Zaldarriaga, M. 2009, MNRAS, 398, 401
- Madau, P., Meiksin, A., & Rees, M. J. 1997, ApJ, 475, 429
- Morales, M. F., Bowmann, J. D., & Hewitt, J. N. 2006, ApJ, 648, 767
- Morales, M. F., & Wyithe, J. S. B. 2010, ARA&A, 48, 127
- Paciga, G., Chang, T. -C., Gupta, Y., et al. 2011, MNRAS, 413, 1174
- Pen, U. -L., Chang, T. -C., Hirata, C. M., et al. 2009, MNRAS, 399, 181
- Petrovic, N., & Oh, S. P. 2011, MNRAS, 413, 2103
- Pritchard, J. R., & Loeb, A. 2012, Rep. Prog. Phys., 75, 086901
- Santos, M. G., Cooray, A. & Knox, L. 2005, ApJ, 625, 575
- Vernstrom, T., Scott, D., & Wall, J. V. 2011, MNRAS, 415, 3641
- White, M., Carlstrom, J. E., Dragovan, M., & Holzapfel, W. L. 1999, ApJ, 514, 12
- Wilman, R. J., Miller, L., Jarvis, M. J., et al. 2008, MNRAS, 388, 1335
- Zaldarriaga, M., Furlanetto, S. R., & Hernquist, L. 2004, ApJ, 608, 622
- Zaroubi, S. 2012, arXiv:1206.0267
- Zheng, Q., Wu, X. -P., Gu, J. -H., Wang, J., & Xu, H. 2012, MNRAS, 424, 2562

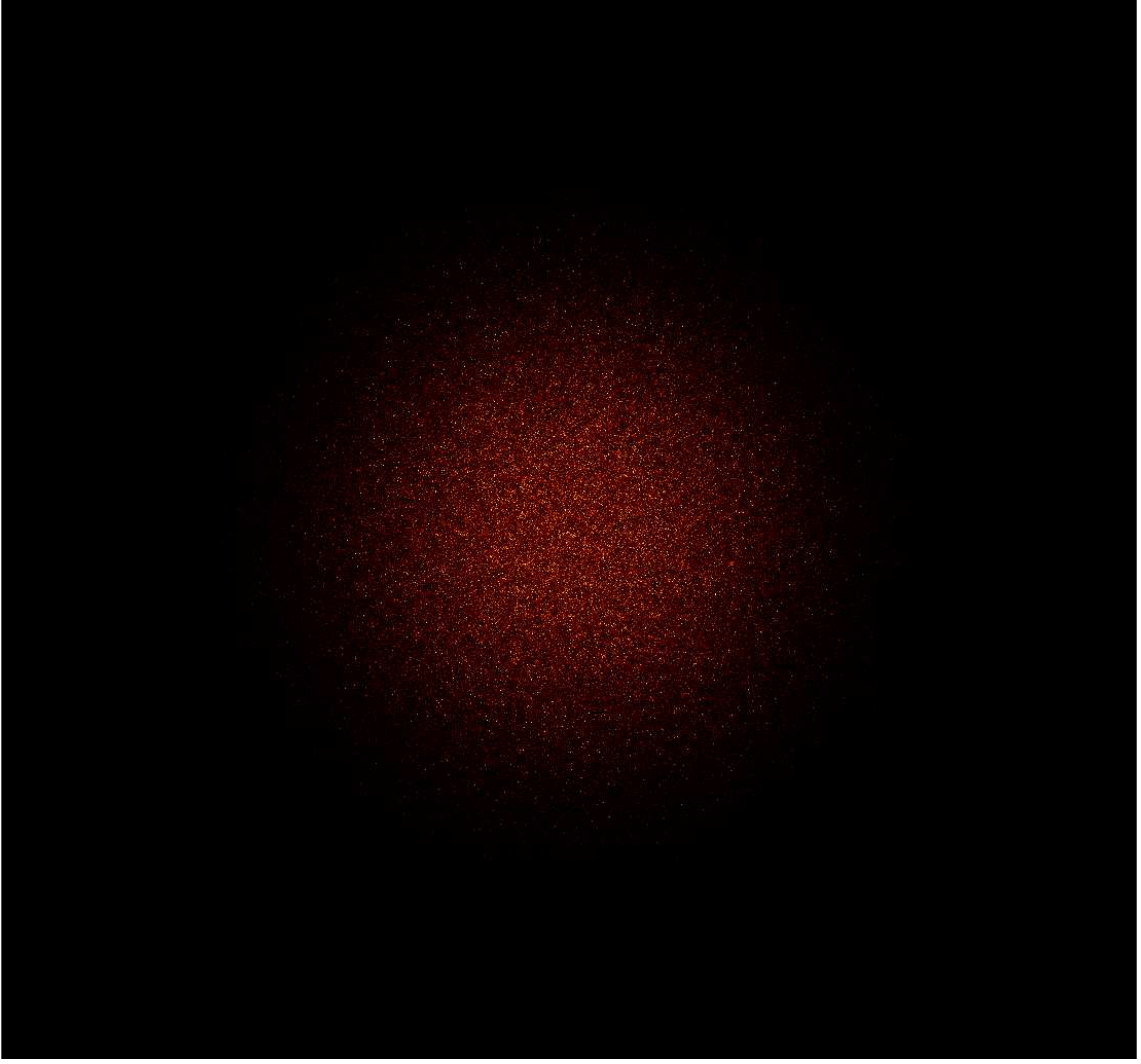


FIG. 1.— Simulated sky map of $20^\circ \times 20^\circ$ at $\nu = 100$ MHz convolved with the 21CMA antenna primary beam. All the bright sources of $S_{150\text{MHz}} \geq 10$ mJy have been removed.

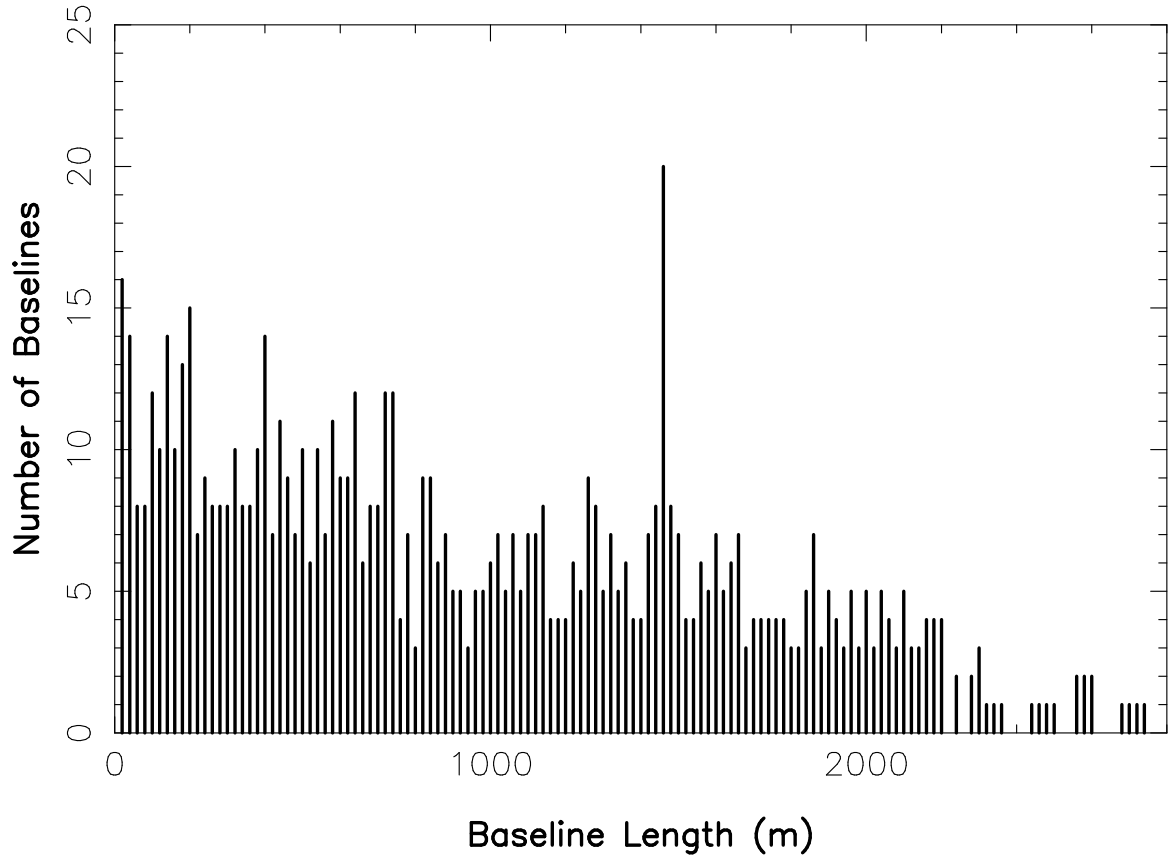


FIG. 2.— Baseline distribution of the 780 pod pairs as interferometers in the 21CMA east-west arm, which also illustrates the uv sampling density when the horizontal axis is scaled in units of observing wavelength. Note that there are only 127 independent baselines among the 780 pairs.

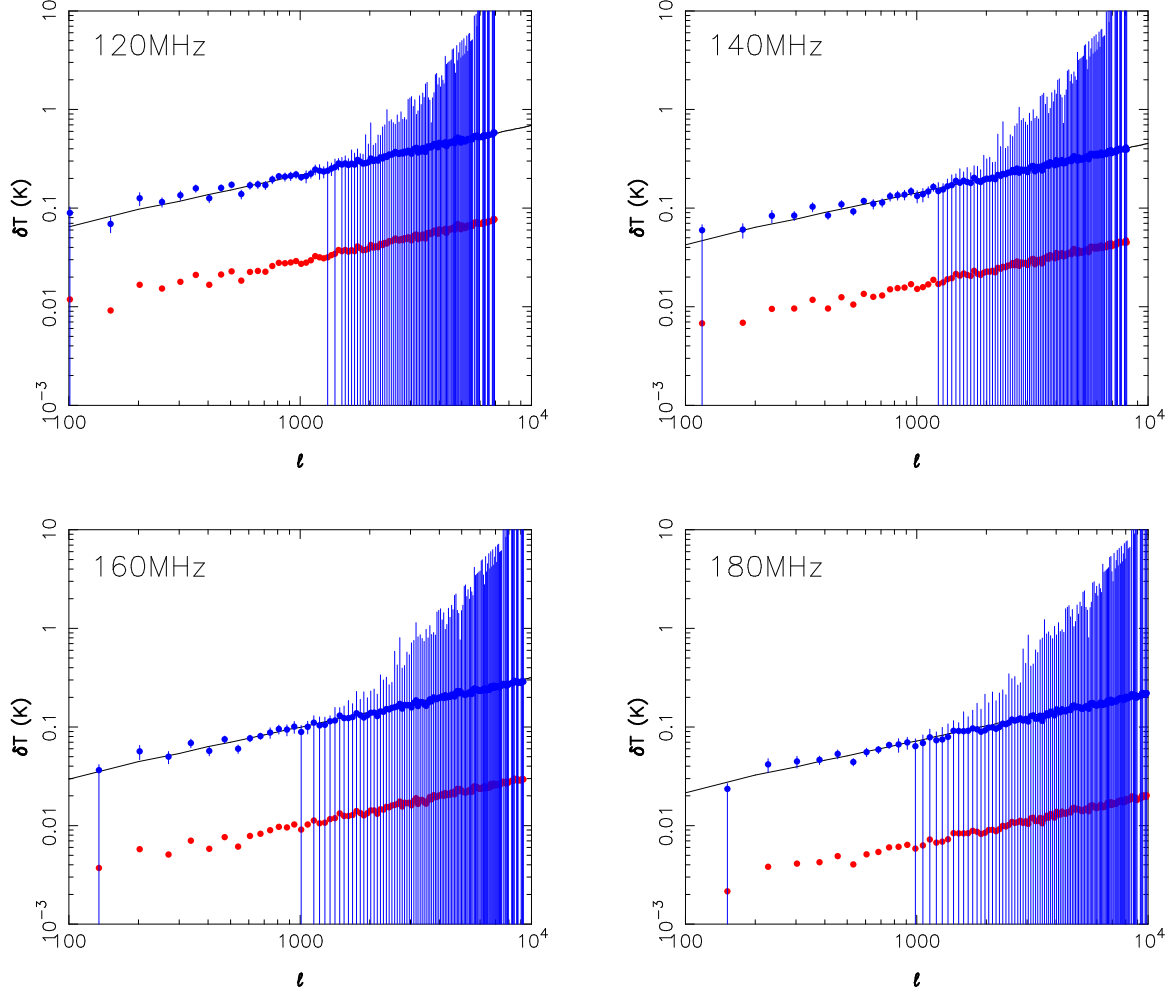


FIG. 3.— Angular power spectra of the simulated sky maps at four frequencies ranging from 120 MHz to 180 MHz, represented by $\delta T = [\ell(2\ell + 1)C_\ell/4\pi]^{1/2}$. Solid lines are the results derived from the simulated maps without any observational and instrumental effects; blue circles are the reconstructed δT , in terms of the visibility correlation coefficients, measured at the 21CMA east-west independent baselines. For comparison the angular power spectra constructed directly from Fig.1 are also shown (red circles), in which the Gaussian beam results in a decrease of the amplitude but does not alter the overall shape of δT .